JOURNAL OF MATERIALS SCIENCE 31 (1996) 4165–4169

Structure evolution in the Cu–Fe system during mechanical alloying

J. Y. HUANG, A. Q. HE, Y. K. WU, H. Q. YE, D. X. LI
Laboratory of Atomic Imaging of Solids, Institute of Metal Research, Academia Sinica, Shenyang 110015, People's Republic of China

High-resolution electron microscopy was used to examine the structure evolution of Cu–60 at % Fe powder mixture during mechanical alloying. Fracture and refinement of particles, the lamellar structure formed by cold-welding, and nanocrystals, were all observed at atomic scale. The X-ray diffraction patterns show that the Bragg peaks from the b c c phase decrease obviously in intensity after 3 h milling and entirely disappear after 5 h milling. Lattice images of the products obtained after 3 h milling reveal that there are Nishiyama–Wasserman orientation relationships between the b c c and f c c phases, i.e. $(0\,0\,1)_\alpha//(1\,1\,0)_\gamma$, $[1\,\bar{1}\,0]_\alpha//[1\,\bar{1}\,2]_\gamma$ and $[1\,1\,0]_\alpha//[\bar{1}\,1\,1]_\Gamma$. It is likely that for a mechanically alloyed iron-rich powder mixture, ball milling induces a reverse martensitic transformation of b c c Fe(Cu) to f c c Fe(Cu) phase. The greatly extended f c c phase range is closely related to this transformation. After 5 h milling, nanocrystals with sizes about 10 nm are formed.

1. Introduction

The technique of mechanical alloying (MA) has been used extensively in recent years to synthesize non-equilibrium phase and states, such as amorphous, quasicrystalline and nanocrystalline materials [1–4]. The phase formation by MA of binary systems with a large negative enthalpy of mixing is now quite well understood [5], but little is known about the phase formation by MA in systems with a small negative enthalpy or positive enthalpy of mixing. The immiscible Cu–Fe system is an example of the latter case [6]. By MA, the solid solubility in the Cu–Fe system has been extended obviously [7–9], but only a few reports [10] concerning the processing mechanism were published and did not satisfactorily explain the obvious extension of f c c phase range.

In this work, high-resolution electron microscopy (HREM) was employed to study the fine structure changes at atomic scale during MA in the Cu–Fe system and a transformation mechanism of b c c to f c c phase induced by ball milling was proposed to explain the great extension of the f c c phase range.

2. Experimental procedure

Elemental copper (with purity of 99.9%) and iron (with purity of 98%) powders with particle sizes of $< 70\,\mu m$ and with overall compositions of $Cu_XFe_{(100-X)}$ ($X = 0$, 15, 20, 35, 40, 50, 100 atom ratio) were mechanically alloyed in a WL-1 planetary ball mill in an argon atmosphere using hardened balls and vials. The ball to powder weight ratio was 20:1. Following milling for various times, a few powders were removed from the vials for analysis. X-ray diffraction (XRD) was performed with a Rigaku diffractometer using CuK_α radiation ($\lambda = 0.1542$ nm). It is quite difficult to make specimens for HREM observations because the particle size of the mechanically alloyed powders is not suitable for direct observation by high-resolution electron microscopy. If the powders are consolidated by hot compaction or by extrusion, their original structures during the MA process would be changed, so one could not really reveal the structure evolution of the MA process. In the present experiment, we invented a new technique of specimen preparation for electron microscopy. The mechanically alloyed powders were mixed in a small amount of epoxy resin; then a piece of metal net (diameter 3 mm) was covered with the mixtures. The as-prepared sample was solidified for a few hours, and then mechanically ground until the metal net was revealed. Finally, the metal net was dimpled and thinned by an argon-ion beam. The original structure information during the process of MA can be shown by means of this technique. The HREM images reported in this paper were all obtained in this way. The HREM observations were made in a Jeol-2000EXII high-resolution electron microscope (accelerating voltage is 200 kV) with an interpretable resolution of about 0.21 nm.

3. Results and discussion

Using XRD patterns of the powder mixture with various compositions for 60 h milling, a metastable phase diagram of the Cu–Fe system can be obtained, as shown in Fig. 1e, and for comparison, the phase ranges obtained from other methods [11, 12] and

other researchers in the Cu–Fe system, are also shown in Fig. 1. It can be seen clearly that thermal evaporation extends the b c c phase range the most, while MA extends the f c c phase range the most. That is, different preparation methods will bring about different solid solubility ranges, which implies that the formation mechanisms of solid solutions are quite different. Even for the same preparation method, for example, on mechanical alloying, the phase ranges still exhibit a little difference, as shown in Fig. 1c,d and e. This is probably caused by the different milling intensity and different ball to powder weight ratios.

Fig. 2 shows that after 3 h milling of $Cu_{40}Fe_{60}$ powder mixture, the diffraction peaks from the b c c phase become weaker and can be hardly seen after 5 h milling. On increasing the milling time up to 60 h, the pattern does not change obviously, but a small displacement of the Bragg peaks from the f c c phase compared with those of pure copper, is observed. These facts indicate that the alloying has occurred after 3 h milling.

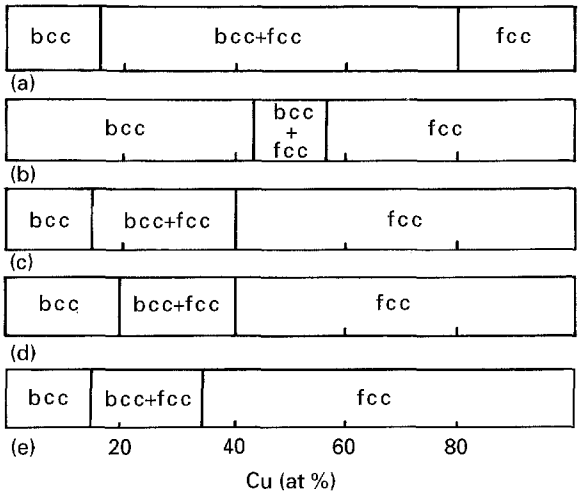

Figure 1 Phase boundaries of $Cu_XFe_{(100-X)}$ alloys obtained by (a) liquid quenching [12], (b) sputtering [11], (c) ball milling [8], (d) ball milling [9], (e) ball-milling (present work).

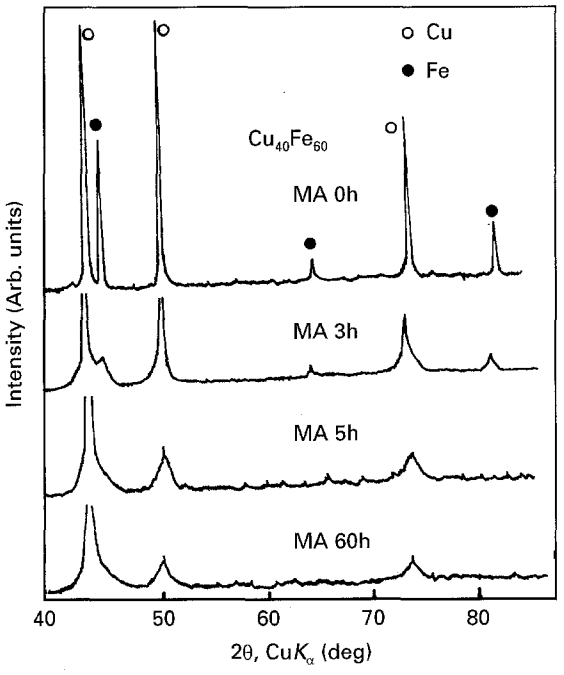

Figure 2 X-ray diffraction patterns for $Cu_{40}Fe_{60}$ after different milling times.

Fig. 3 is a high-resolution (HR) lattice image of crystals with different orientation after 1 h milling. In the upper-left and lower-right part of the photograph, the lattice fringes have been twisted and deviated from the original orientation as indicated by the black line. Dislocations (marked with arrow heads and a circle), twins and heavy distortion areas around the surface of the particles can be seen clearly, the interface (shown as dashed lines) between the two crystals can also be seen. From this it can be understood that many crystal defects have been produced after 1 h MA. Fig. 4a shows the fracture morphology of a particle. The fringe spacing is 0.208 nm, corresponding to a $d_{Cu(1\,1\,1)}$ interplanar spacing, the crack trend which has been indicated by dashed lines, can be clearly seen. The fringe images near the crack have been heavily twisted and dislocations appear continuously. The atoms in the crackle area (between the dashed lines) are disordered. Near the surface of the particle, the crystal has deformed heavily and some clusters can be found (circle 4) composed of a few unit cells, nanocrystals (circle 3) and amorphous-like areas (circles 1, 2). In Fig. 4b, a small copper particle (on the left) has been separated from a larger one (on the right). Further study shows that there is a twin relationship (as shown by the long arrows) between these two particles. From their profiles it can be concluded that the two particles should have originally been one particle, but it had cracked into two parts. It is very possible that firstly the copper particle forms twins along its close-packed planes due to repeated mechanical deformation, and then subsequent milling makes it crack. Microtwins can also be found towards the bottom of the particle (as shown by the short arrows). In Fig. 5, the fringe spacing at the top and bottom part is 0.208 nm corresponding to a $d_{Cu(1\,1\,1)}$ interplanar spacing (f), the crystals between the copper particles is iron (b). This is obviously a lamellar structure (their boundaries are shown with dashed lines), formed due to repeated mechanical deformation and cold-welding. The process of MA is composed of three different stages [13, 14]: during the first stage, MA produces powder particles with a characteristically layered microstructure. Further millings leads to an ultrafine composite.

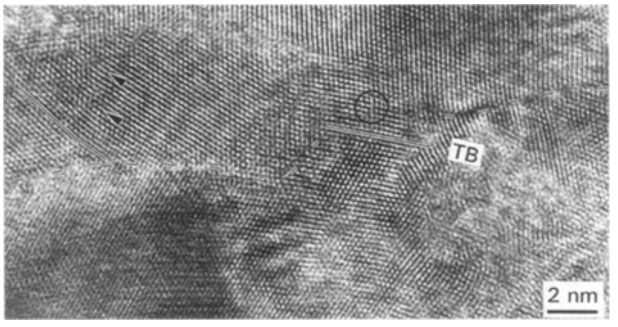

Figure 3 Surface deformation and internal structure defects of $Cu_{40}Fe_{60}$ after 1 h MA. Dislocations, a twin and an interface are marked with arrows, TB and dashed lines, respectively.

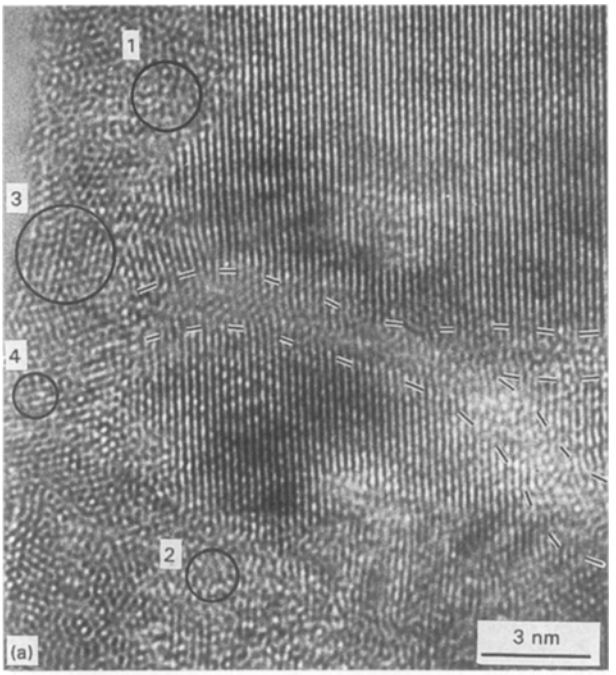

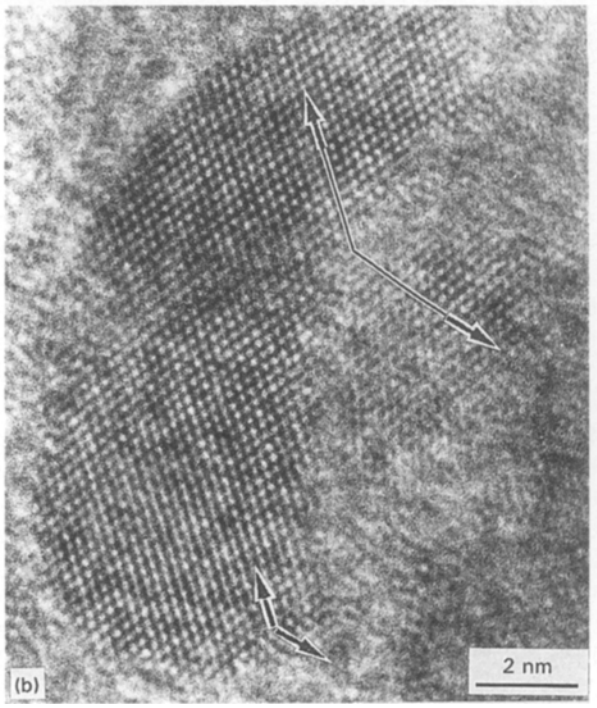

Figure 4 (a) The crack (between the dashed lines), dislocations (arrows), nanocrystals (circle 3), clusters (circle 4) and amorphous-like areas (circles 1,2) of copper particles after 1 h MA. (b) Fracture of a copper particle after 1 h MA.

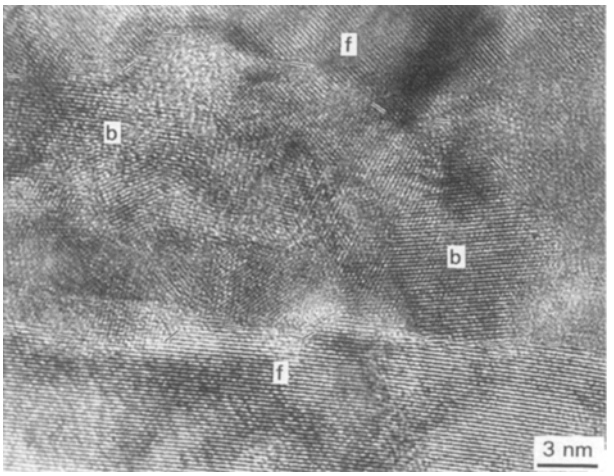

Figure 5 The layered structure formed due to repeated mechanical deformation and cold-welding. F c c and b c c phases are denoted by f and b, respectively.

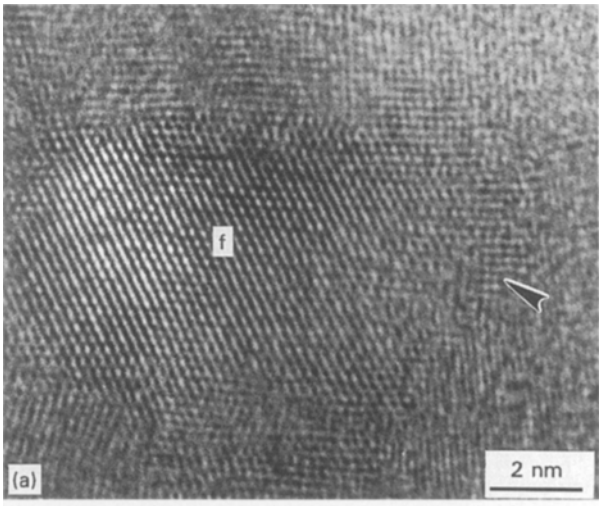

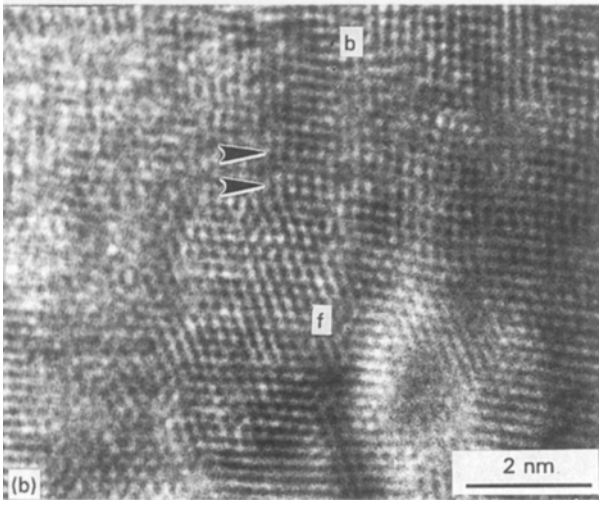

Figure 6 The N–W orientation relationship between (a) the f c c (f) and b c c (arrowheads) phases, and (b) the f c c phase and the transitional structure of the b c c phase (arrowed).

Finally, a true alloying by a solid-state interdiffusion reaction occurs. Obviously Fig. 5 reveals the characteristics of the first stage during MA. Fig. 6 shows two typical high-resolution images of particles after 3 h MA. In Fig. 6a the two-dimensional square network indicated by an arrow having a unit cell of 0.20 nm, corresponds to $\langle 0\,0\,1 \rangle$ lattice image of the b c c phase and the one-dimensional lattice image (f) with a spacing of 0.21 nm correspond to the f c c phase. By detailed examination of Fig. 6a one can see that the upper right part of the f c c phase exhibited two-dimensional lattice imaging morphology. By comparing the two two-dimensional lattice images the well-known Nashiyama–Wasserman (N–W) orientation relationships can be found: $(0\,0\,1)_\alpha // (1\,1\,0)_\gamma$, $[1\,\bar{1}\,0]_\alpha // [1\,\bar{1}\,2]_\gamma$ or $[1\,1\,0]_\alpha // [\bar{1}\,1\,1]_\Gamma$. From this and their morphological characteristics and the X-ray diffraction results, it is reasonable to suppose that this f c c phase resulted from the b c c phase and such a transformation might be inverse martensitic induced

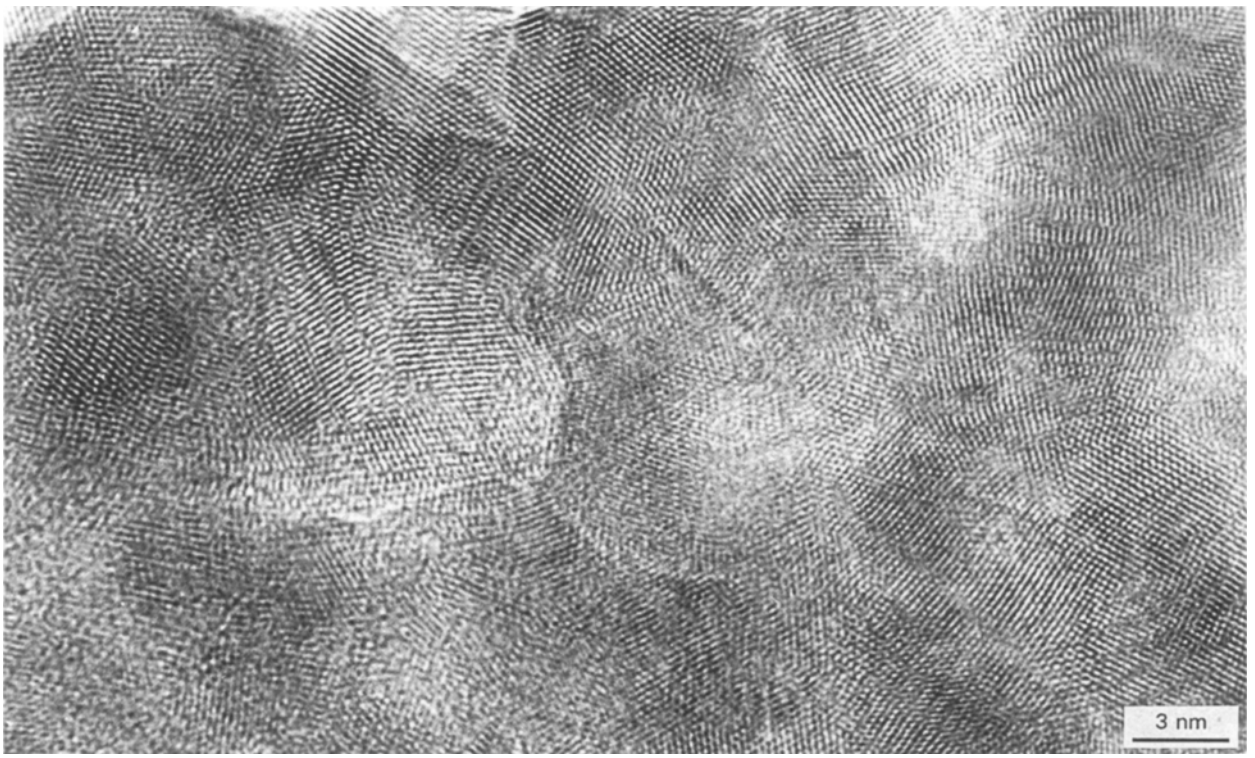

Figure 7 Nanocrystals formed after 60 h MA.

by deformation. In Fig. 6b, a transitional structure consisting of a few distorted square networks, as shown by arrow heads, is seen at the top of the fcc lattice imaging with $\langle 1\,1\,0\rangle$ orientation (f). If the distortion is considered as a kind of shear, the shear system is $\{1\,1\,0\}_{bcc}$ and $\langle 1\,1\,0\rangle_{bcc}$ or $\{1\,1\,1\}_{fcc}$ and $\langle 1\,1\,2\rangle_{fcc}$ using the fcc coordinate system, which is also evidence of martensitic transformation. These results indicated that the reduction of the bcc phase is closely related to the martensitic transformation of bcc phase into fcc phase in addition to the dissolution of iron atoms into fcc phase. As more copper atoms (>15%, for example) dissolve into the bcc phase, the bcc phase will become unstable and under repeated action of an external force it could transform inverse martensitically into fcc phase.

XRD shows that after 5 h milling for the powders of $Cu_{40}Fe_{60}$, bcc peaks have completely disappeared and only fcc peaks remain. At room temperature, copper and iron are almost completely immiscible due to a positive enthalpy of mixing, but during MA an external force causes copper atoms to disperse to iron crystals with more defects and vice versa, as in ion implantation which is not a process of simple chemical diffusion (caused by density gradation). We consider this process to be the onset of MA, a part of the iron is forced to diffuse into copper crystals and a part of the copper into the iron crystals, and when the solubility of copper in iron is sufficient, the α-Fe(Cu) will transform into γ-Fe(Cu), inverse martensitically. When discussing the miscibility gap in Cu–Fe alloys (this alloy was prepared by rapid quenching), Klement [12] pointed out that the copper-rich boundary of the miscibility gap may actually lie at iron concentrations higher than the calculated result due to the diffusionless fcc → bcc transformations. For a similar reason, in our case, the extent of fcc phase range may actually be narrower than the experimental result, because of the diffusionless bcc → fcc transformations. So it is very possible that the products after 5 h MA are composed of two parts: one is copper-based solid solution Cu(Fe), the other is iron-rich γ-phase. Both of them are fcc structure and the difference between their lattice parameters is too slight to be distinguished by XRD or electron diffraction, but their components are very different. Subsequent milling only makes them homogeneous. After 60 h of MA, homogeneous nanocrystals with many defects are formed. The average grain sizes, calculated from the broadening of the XRD peaks, vary between 10 and 20 nm which is consistent with the grain sizes of Fig. 7 obtained by HREM.

4. Conclusions

After 5 h milling for the powders of $Cu_XFe_{(100-X)}$ ($X = 0$, 5, 15, 20, 35, 40, 50, 100 atomic ratio), three phase regions appear: single-phase bcc alloys form for $X < 15$ and single-phase fcc alloys form for $X > 35$, both phases coexist for $15 < X < 35$. HREM observations for the powders of $Cu_{40}Fe_{60}$ shows that during MA bcc phase transforms to fcc phase following an N–W orientation relationship, and this transformation may be inverse martensitic, to which the solubility extension of the fcc phase is related. Also the fracture and refinement of particles, clusters, nanocrystals and cold-welding images were clearly detected at the atomic scale. After 60 h milling, homogeneous nanocrystals with a grain size of about 10–20 nm are formed.

Acknowledgement

This work was supported by the National Science Foundation of China under grant numbers of 59271011 and 59371008 which is gratefully acknowledged.

References

1. R. B. SCHWARZ and C. C. KOCH, *Appl. Phys. Lett.* **49** (1986) 146.
2. J. ECKERT, L. SHULTZ and K. URBAN, *ibid.* **55** (1988) 117.
3. E. HELLSTERN, H. J. FECHT, Z. FU and W. L. JOHNSON, *J. Appl. Phys.* **65** (1988) 305.
4. J. ECKERT, J. C. HOLZER, C. E. KRILL III and W. L. JOHNSON, *J. Mater. Res.* **7** (1992) 1751.
5. L. SCHULTZ, *Mater. Sci. Eng.* **97** (1988) 15.
6. T. B. MASSALSKI (ed.), "Binary Alloys Phase Diagram", 2nd Edn, (ASM International, Metals Park, OH, 1990) p, 1408.
7. K. UENISHI, K. F. KOBAYASHI, S. NASU, H. HATANO, K. N. ISHIBARA and P. H. SHINGU, *Z. Metalkde* **83** (1992) 132.
8. Y. Z. YANG, X. M. MA and Y. D. DONG, *Acta Metall. Sinica* **28** (1992) A399.
9. J. ECKERT, J. CHOLZER, C. E. KRILL III and W. L. JOHNSON, *J. Mater. Res* **7** (1992) 1980.
10. A. R. YAVARI, P. J. DESRE and T. BENAMEUR, *Phys. Rev. Lett.* **68** (1992) 2235.
11. K. SUMIYAMA, T. YOSHITAKE and Y. NAKAMURA, *J. Phys. Soc. Jpn* **53** (1984) 3160.
12. W. KLEMENT JR, *Trans. AIME* **233** (1965) 1180.
13. R. B. SCHWARZ, C. K. PETRICH and C. K. SAW, *J. Non-Cryst. Solids* **76** (1985) 281.
14. E. HELLSTERN and L. SCHULTZ, *Appl. Phys. Lett.* **48** (1986) 124.

Received 17 December 1993
and accepted 1 December 1995